Journal of Power Sources 196 (2011) 3855–3862

Contents lists available at ScienceDirect

Journal of Power Sources

journal homepage: www.elsevier.com/locate/jpowsour

A new Gd-promoted nickel catalyst for methane conversion to syngas and as an anode functional layer in a solid oxide fuel cell

Wei Wang, Chao Su, Ran Ran, Zongping Shao*

State Key Laboratory of Materials-Oriented Chemical Engineering, College of Chemistry & Chemical Engineering, Nanjing University of Technology, No. 5 Xin Mofan Road, Nanjing 210009, PR China

ARTICLE INFO

Article history:
Received 19 November 2010
Received in revised form
16 December 2010
Accepted 16 December 2010
Available online 24 December 2010

Keywords:
Solid-oxide fuel cells
Nickel–alumina
Anode catalyst layer
Methane
Carbon deposition
Lanthanide promotion

ABSTRACT

The effect of lanthanide promoters on a Ni–Al_2O_3 catalyst for methane partial oxidation, steam reforming and CO_2 reforming at 600–850 °C is systematically investigated. The promoters include La_2O_3, CeO_2, Pr_2O_3, Sm_2O_3 and Gd_2O_3. GdNi–Al_2O_3 shows comparable catalytic activity to LaNi–Al_2O_3 and PrNi–Al_2O_3 but higher activity than CeNi–Al_2O_3 and SmNi–Al_2O_3 for all three reactions. The O_2-TPO results show that GdNi–Al_2O_3 possesses the best coke resistance among those tested. It also displays good stability at 850 °C for 300 h. Raman spectroscopy indicates that the addition of lanthanide promoters can reduce the degree of graphitization of the carbon deposited on Ni–Al_2O_3. The GdNi–Al_2O_3 is further applied as an anode functional layer in solid-oxide fuel cells operating on methane. The cell yields peak power densities of 1068, 996 and 986 mW cm^{-2} at 850 °C, respectively, for operating on methane–O_2, methane–H_2O and methane–CO_2 gas mixtures, which is comparable to operating on hydrogen fuel. GdNi–Al_2O_3 is promising as a highly coking-resistant catalyst layer for solid-oxide fuel cells.

1. Introduction

As the main component of natural gas, coal-bed gas and biogas with huge reserves, methane is a clean fuel and also an important raw material for the synthesis of many important chemicals such as hydrogen and methanol. The conversion of methane to synthesis gas (syngas), a mixture of CO and H_2, is an important step toward the utilization of methane in chemical synthesis. Syngas can be produced from methane by catalytic partial oxidation ($CH_4 + 1/2O_2 = CO + 2H_2$, $\Delta H_{298\,K} = -36\,kJ\,mol^{-1}$), steam reforming ($CH_4 + H_2O = CO + 3H_2$, $\Delta H_{298\,K} = 206\,kJ\,mol^{-1}$), or CO_2 reforming ($CH_4 + CO_2 = 2CO + 2H_2$, $\Delta H_{298\,K} = 247\,kJ\,mol^{-1}$). The above three reactions create products with different H_2 to CO ratios and are suitable for the synthesis of different chemicals [1].

Fuel cells are electrochemical devices that can directly convert chemical energy to electrical power with high efficiency and low emissions. Among the many types of fuel cells, solid oxide fuel cells (SOFCs), which typically operate at 500–1000 °C, have received particular attention recently. The elevated operational temperature allows for fuel flexibility. In principle, SOFCs can operate on any combustible fuel [2–6]. As the simplest hydrocarbon, methane is considered to be an attractive fuel for SOFCs because it has several advantages such as ease and safety of storage and also being handled and delivered with the existing supply infrastructure. Nickel cermets are the most commonly used anodes in hydrogen-fueled SOFCs due to their high electrochemical activity for hydrogen electro-oxidation and long-term stability at SOFC operating conditions [7,8]. However, they suffer from a number of drawbacks when operating on hydrocarbon fuels, notably carbon deposition, which covers the active sites of the anodes and causes rapid and irreversible cell deterioration. To overcome those disadvantages, substantial efforts have been devoted to the development of new non-nickel anode materials in recent years [9–12]. The most investigated materials include copper-based cermet and perovskite-type oxides. However, those materials decreased not only the carbon deposition rate but also the electrochemical activity for hydrocarbon oxidation. The modification of conventional nickel cermet anodes has also been tried and is more advisable due to its simplicity. Recently, the Barnett group successfully directly operated SOFCs with a conventional nickel cermet anode on methane, propane and other hydrocarbons without pre-reforming by modification of the anode with a Ru–CeO_2 functional layer [13–15]. However, Ru is expensive, making it less attractive for practical applications.

Some supported group VIII metals are known to be good catalyst candidates for methane conversion reactions to give a high yield of syngas at elevated temperatures [16–20]. Very recently, we have demonstrated that a cost-effective Ni–Al_2O_3 catalyst presented

* Corresponding author. Tel.: +86 25 8317 2256; fax: +86 25 8317 2256.
E-mail address: shaozp@njut.edu.cn (Z. Shao).

0378-7753/$ – see front matter © 2010 Elsevier B.V. All rights reserved.
doi:10.1016/j.jpowsour.2010.12.072

good catalytic activity comparable to Ru–CeO_2. When operating on methane-containing fuels, the fuel cell with a Ni–Al_2O_3 anode functional layer yielded high power output comparable to that with hydrogen. In addition, the Ni–Al_2O_3 catalyst layer showed much better thermal–mechanical compatibility with the cermet anode than Ru–CeO_2 [21,22].

As mentioned, one practical problem with a nickel-based catalyst is the coke-induced deactivation. It is thought that metal oxides alter the activity of the supported metal catalysts depending on the nature of the additives. Catalyst modification can cause the blockage of active sites on the metal surface or changes in the electronic character or geometric structure of the catalyst surface, thus changing the reactivity by interacting with the substrate to alter its mode of adsorption [23]. There is evidence in the literature indicating an improvement in the catalytic activity of Ni-based catalysts in hydrocarbon steam/CO_2 reforming and partial oxidation with the addition of lanthanide elements [24–30]. Zhuang et al. and Wang et al. have investigated the effect of cerium oxide as a promoter in supported Ni catalysts for methane steam and CO_2 reforming [24,25]. There was a beneficial effect with not only a decrease in the carbon deposition rate but also an increase in the reforming activity. The researchers believed that the cerium oxide accelerated the reaction of steam with the adsorbed species on the nickel surface and thus decreased the carbon deposition rate as well as increased or maintained the high catalytic activity. Yang et al. have reported that La_2O_3 and CeO_2 co-promoted Ni–Al_2O_3 catalyst for the methane CO_2 reforming reaction. Not only was the amount of carbon deposition decreased, but the activity was also improved slightly using the Ni/γ-Al_2O_3 with the La_2O_3–CeO_2 binary promoters, due to the alkaline function and dispersion action of La_2O_3–CeO_2 as well as the electronic interactions between CeO_2 and Ni [31].

In our previous work, we have demonstrated that a lithium and lanthanum co-promoted Ni–Al_2O_3 catalyst has an excellent catalytic activity for the partial oxidation, steam and CO_2 reforming of methane between 600 and 850 °C and good coking resistance and operational stability [32]. In this study, the effect of lanthanide promoters on the catalytic activity of the Ni–Al_2O_3 catalyst for methane reforming and partial oxidation reactions and coke resistance was systematically investigated. The Gd-modified Ni–Al_2O_3 catalyst was further investigated as an anode functional layer operating under real fuel cell conditions with methane as the fuel.

2. Experimental

2.1. Synthesis and fabrication

All of the catalyst powders were synthesized using a glycine nitrite process (GNP), which was described previously [33]. The resultant primary powders from the direct combustion were further calcined at 850 °C for 5 h in static air to obtain the desired catalysts. After cooling to room temperature, the powder was pressed into disk-shaped pellets and then crushed to small grains with the desired particle size for the catalytic tests.

The fuel cell materials included a $La_{0.8}Sr_{0.2}MnO_3$ (LSM) cathode, a $(Y_2O_3)_{0.1}(ZrO_2)_{0.9}$(YSZ) electrolyte and a NiO + YSZ anode (NiO:YSZ = 60:40, by weight). The LSM was synthesized using a standard combined EDTA–citrate complexing sol–gel process with metal nitrates (analytical reagents) applied as the raw materials [34], while the NiO and YSZ used for the anode were commercial products (Chengdu Shudu Nano-science Co., Ltd. for NiO and Tosoh for YSZ). The disk-shaped anode substrates were first prepared using a tape-casting technique. The green anode pellets were fired at 1100 °C for 2 h in air to release the organic solvents and to create the proper mechanical strength for the substrate. The YSZ colloidal suspension was prepared by dispersing a fine YSZ powder into a solution of ethylene glycol (5 wt.% solids content) through high-energy ball milling (Fritsch, Pulverisette 6), which was then spray deposited onto the anode substrates. The obtained green anode–electrolyte dual layer half-cells were sintered at 1400 °C for 5 h in air. The LSM + YSZ composite cathode (70:30, by weight) was deposited on the sintered electrolyte surface and then fired at 1100 °C for 2 h in air. To prepare the catalyst layer, a slurry of the catalyst powder was first prepared and then was screen-painted onto the outer surface of the anode layer and sintered at 850 °C for 1 h.

2.2. Catalytic evaluation

The catalytic activity of the lanthanide-promoted Ni–Al_2O_3 catalysts was tested in a flow-through type fixed-bed quartz-tube reactor with an inner diameter of about 8 mm. About 0.2 g of the catalyst particles in the size range of a 40–60 mesh were placed into the middle of the reactor. The gas mixtures were fed into the reactor at the flow rates of $CH_4/O_2/He = 10/5/80$, $CH_4/H_2O/He = 10/10/80$ and $CH_4/CO_2/He = 10/10/80$ ml min^{-1} [STP] for the partial oxidation, steam reforming and CO_2 reforming of methane, respectively. The gases, controlled by AFC 80MD digital mass flow controllers (Qualiflow), were introduced to the top of the reactor. Compositional analysis of the effluent gases from the bottom of the reactor was performed with a Varian 3800 gas chromatograph, which was equipped with Hayesep Q, Poraplot Q and 5 Å sieve molecular capillary columns and a thermal conductivity detector (TCD) for the separation and detection of H_2, O_2, CO, CO_2 and CH_4. The catalytic reactions were performed at 600–850 °C. The conversion of methane (X(%)) during the partial oxidation and steam reforming of methane was calculated according to Eq. (1). Alternatively, the conversion of methane during CO_2 reforming was calculated according to Eq. (2), and the selectivity of CO (S(%)) was calculated according to Eq. (3). The H_2 to CO ratios (R) were calculated according to Eqs. (4)–(6) for partial oxidation, steam reforming and CO_2 reforming of methane, respectively:

$$X(\%) = \frac{[CO] + [CO_2]}{[CO] + [CO_2] + [CH_4]} \times 100\% \quad (1)$$

$$X(\%) = \frac{0.5 \times [CO]}{0.5 \times [CO] + [CH_4]} \times 100\% \quad (2)$$

$$S(\%) = \frac{[CO]}{[CO] + [CO_2]} \times 100\% \quad (3)$$

$$R = \frac{4}{S_{[CO]}\%} - \frac{1}{S_{[CO]}\% \times X_{[CH_4]}\%} - 1 \quad (4)$$

$$R = \frac{4}{S_{[CO]}\%} - 1 \quad (5)$$

$$R = \frac{4 \times X_{[CH_4]}\%}{S_{[CO]}\% + S_{[CO]}\% \times X_{[CH_4]}\%} - 1 \quad (6)$$

2.3. Characterizations

Hydrogen temperature-programmed reduction (H_2-TPR) was used to identify the chemical interaction between the nickel and the support and/or the promoters. Approximately 0.03 g of catalyst particles were put in a U-type quartz reactor with an inner diameter of about 3 mm. The sample was pretreated under a pure argon atmosphere at a flow rate of 30 ml min^{-1} [STP] at 400 °C for 30 min. After cooling to room temperature, the atmosphere was switched to 10 vol.% H_2/Ar, and the reactor was programmatically heated to 930 °C at a rate of 10 °C min^{-1}. The hydrogen consumption was monitored by an in situ TCD detector with a BELCAT-A apparatus.

To test the coke resistance of the lanthanide-promoted Ni–Al_2O_3 catalysts, about 0.2 g of catalyst particles were first placed in a flow-through type quartz-tube reactor and treated at 850 °C under a pure methane atmosphere at a flow rate of 40 ml min^{-1} [STP] for 5 min and then cooled to room temperature in a helium atmosphere. After the treatment, approximately 0.05 g of powder was placed into a U-type quartz reactor with an inner diameter of about 3 mm. Pure oxygen (for oxygen temperature-programmed oxidization, O_2-TPO) at a flow rate of 20 ml min^{-1} [STP] was then introduced to the top of the reactor. After flowing with the gas at room temperature for about 30 min to stabilize the baseline, the reactor was heated to 800 °C at a rate of 10 °C min^{-1}. The deposited carbon on the catalyst surface was gradually oxidized to CO_2. The effluent gas from the reactor was connected to a mass spectrometer (MS, Hiden QIC-20) for in situ monitoring of CO_2.

The CO_2-TPD process was performed to test the surface basicity of the catalysts. The samples were first reduced in hydrogen at 850 °C for 1 h, cooled to room temperature, and then exposed to CO_2 (20 ml min^{-1}) for 2 h. The treated samples were purged with Ar at room temperature for 1 h and heated linearly at 10–800 °C in a flowing Ar atmosphere at 20 ml min^{-1}. The CO_2 signal was monitored and recorded continuously as a function of the temperature by the MS.

The phase structures of the various samples were examined using an X-ray diffractometer (XRD, ARL X' TRA) equipped with a Cu Kα radiation (λ = 0.1541 nm). The BET specific surface area of the catalysts was characterized by N_2 adsorption at liquid nitrogen temperature using a surface area analyzer (BELSORP II, Japan). Prior to nitrogen adsorption, the sample was degassed at 300 °C for 2.0 h to remove any physically adsorbed species. The surface area was determined from the linear portion of the BET equation. The laser Raman spectroscopy of the various catalysts after treated at 850 °C under a pure CH_4 atmosphere for 5 min was obtained in an HR800 UV Raman microspectrometer (JOBIN YVON, France) using the green line of an argon laser (λ = 514.53 nm) as the excitation source. The cross-sectional morphologies of the fuel cells were examined using an environmental scanning electron microscope (ESEM, QUANTA-200).

The *I–V* polarization curves of the fuel cells measured at 650–850 °C were obtained using a Keithley 2420 source meter in 4-probe mode. During the measurements, hydrogen, CH_4–O_2, CH_4–H_2O or CH_4–CO_2 gas mixtures were fed into the anode chamber and ambient air was served as the oxidant gas at in the cathode chamber. The flow rate of hydrogen and methane was maintained at 80 ml min^{-1} [STP].

3. Results and discussion

3.1. Basic properties

The development of active and stable catalysts for methane conversion to syngas is critical for methane utilization in chemical synthesis. On the other hand, an ideal material for the anode functional layer of SOFCs operating on methane should possess high activity for all three reactions (partial oxidation, steam reforming and CO_2 reforming of methane) because the CO_2, and H_2O could co-present with the methane under polarization by introducing methane and oxygen as the anode feed gases. We have previously demonstrated that a Ni–Al_2O_3 (7 wt.% Ni) catalyst prepared by a glycine nitrate combustion process had good activity for the afore-mentioned three reactions at intermediate temperatures. To further improve the catalytic performance, a series of lanthanides (La_2O_3, CeO_2, Pr_2O_3, Sm_2O_3 and Gd_2O_3) were applied as promoters to modify the Ni–Al_2O_3 catalyst. Five new catalysts, i.e., LaNi–Al_2O_3, CeNi–Al_2O_3, PrNi–Al_2O_3, SmNi–Al_2O_3 and GdNi–Al_2O_3 were prepared by the same combustion method, and for comparison, Ni–Al_2O_3 was also synthesized. In all six catalysts, the nickel content was fixed at 15 wt.% and the molar ratio of promoters to nickel was fixed at 0.12:1. The contents of the promoters were 5.00, 5.28, 5.06, 5.35 and 5.56 wt.% for LaNi–Al_2O_3, CeNi–Al_2O_3, PrNi–Al_2O_3, SmNi–Al_2O_3 and GdNi–Al_2O_3, respectively. It is interesting that all of the catalysts were light blue in color except for the CeNi–Al_2O_3, which was light green. The XRD results are shown in Fig. 1. As shown, the γ-Al_2O_3 and $NiAl_2O_4$ phases were detected in all of the samples. No other phase like NiO was observed in the LaNi–Al_2O_3, PrNi–Al_2O_3, SmNi–Al_2O_3 and GdNi–Al_2O_3. These results suggest that the La, Pr, Sm and Gd oxides were all well-dispersed within the catalysts. However, the CeO_2 phase was detected in the CeNi–Al_2O_3, which agreed well with the literature [31,35]. This result implies that CeO_2 likely did not enter into the bulk phase of the Ni–Al_2O_3 catalysts. The existence of the yellowish-color CeO_2 should explain the green color of CeNi–Al_2O_3.

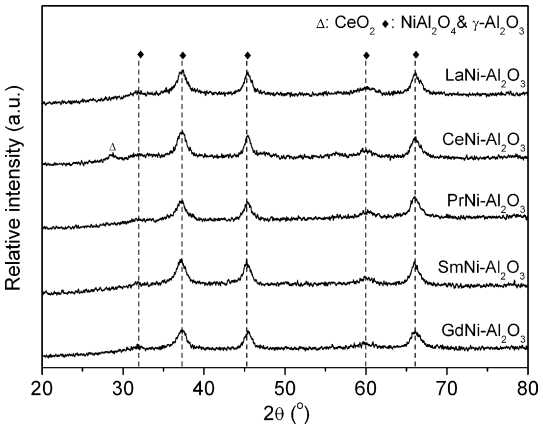

Fig. 1. The XRD patterns of the various catalysts after calcination at 850 °C.

The specific surface areas were determined using the nitrogen adsorption method at the liquid nitrogen temperature and were 51.3, 69.5, 79.0, 52.7, 56.2 and 68.3 $m^2 g^{-1}$ for LaNi–Al_2O_3, CeNi–Al_2O_3, PrNi–Al_2O_3, SmNi–Al_2O_3, GdNi–Al_2O_3 and Ni–Al_2O_3, respectively. These findings indicate that the promoters affected the specific surface area of the catalysts. It has been reported that a maximum BET surface area of La_2O_3/Al_2O_3 composites exists, changing with the La_2O_3 loading (La/Al ratio). However, the La/Al ratio having the maximum BET value varies between investigations depending on the different preparation conditions [36,37]. Chen et al. found that the specific surface area of the La_2O_3-promoted Al_2O_3 samples was higher than that of the pure Al_2O_3 sample when La/Al ≤ 0.02 and that the maximum specific surface area was achieved at a La/Al atomic ratio of 0.02. For La/Al ≥ 0.05, the specific surface areas of the La_2O_3-promoted aluminum samples decreased rapidly with the increase in the La/Al atomic ratio [36]. Roh et al. also reported that the largest specific surface area of a LaNi–Al_2O_3 catalyst was obtained at the La/Al atomic ratio of 0.02 [38], while Haack et al. have reported that the maximum specific surface area was achieved at a La/Al atomic ratio of 0.15 [37]. In this study, the specific surface area of LaNi–Al_2O_3 (La/Al = 0.022) was relatively smaller than that of Ni–Al_2O_3, which was different from the literature cited above. This phenomenon may be attributable to the different preparation method we used in this study. The specific surface area of the CeNi–Al_2O_3 was very close to the Ni–Al_2O_3. Wang et al. have demonstrated the effect of different cerium contents on the specific surface areas of the CeO_2-promoted Ni–Al_2O_3 catalysts, and the specific surface area of Ni–1 wt.% CeO_2–Al_2O_3 was slightly higher than that of the unpromoted Ni–Al_2O_3 catalyst, while Ni–5 wt.% CeO_2–Al_2O_3 has about the same specific surface

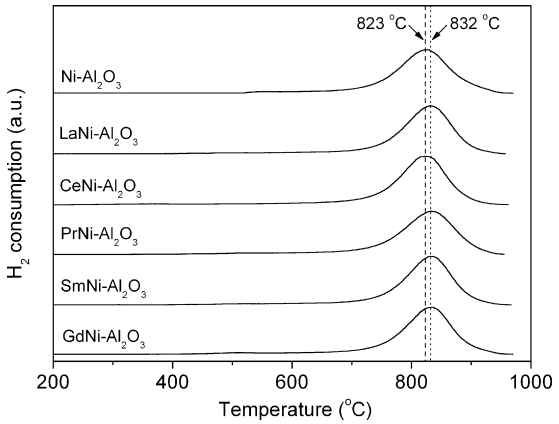

Fig. 2. The H_2-TPR profiles of the LaNi–Al_2O_3, CeNi–Al_2O_3, PrNi–Al_2O_3, SmNi–Al_2O_3, GdNi–Al_2O_3 and Ni–Al_2O_3 catalysts.

area as that of Ni–Al_2O_3 [25]. In this study, the content of CeO_2 was 5.28 wt.%, and thus, the surface area results agree well with the literature. Guo et al. have reported on the effect of the Gd_2O_3 content on the BET surface area in a Ni–SiO_2 system [39]. The authors believed that the surface area of Ni–SiO_2 decreased with the addition of Gd_2O_3. Our results with the Gd-promoted Ni–Al_2O_3 catalyst showed the same trend as their observations, although the supports were different.

The chemical interaction between the nickel and the support and/or the promoters was characterized by H_2-TPR. Fig. 2 shows the H_2-TPR profiles of the various catalysts. The reduction peak temperature of the free NiO during the H_2-TPR process was reported to be around 330 °C [40]. With the increase in the chemical interaction between the NiO and the support or promoters, a shift of the reduction peak to higher temperatures was expected. The reduction peak temperatures of the six catalysts were all higher than 800 °C, suggesting a strong interaction between the nickel and the support (γ-Al_2O_3) or the promoters in the various catalysts synthesized by the GNP method. Such interaction could effectively suppress the grain growth of the NiO phase that is beneficial for increasing the catalytic activity of the catalysts. The peak temperatures were 832, 823, 832, 832, 833 and 823 °C for the LaNi–Al_2O_3, CeNi–Al_2O_3, PrNi–Al_2O_3, SmNi–Al_2O_3, GdNi–Al_2O_3 and Ni–Al_2O_3, respectively. These findings indicate that the lanthanide additives could affect the metal-support interaction with the exception of the CeO_2 additive. The same peak reduction temperatures of CeNi–Al_2O_3 and Ni–Al_2O_3 can be explained by the lack of a strong chemical interaction between the CeO_2 and the support as demonstrated by the XRD.

3.2. Catalytic performance

Fig. 3 shows the methane conversion and CO selectivity for the LaNi–Al_2O_3, CeNi–Al_2O_3, PrNi–Al_2O_3, SmNi–Al_2O_3 and GdNi–Al_2O_3 catalysts for the partial oxidation, steam reforming and CO_2 reforming of methane with the methane to O_2, H_2O and CO_2 ratios of 2:1, 1:1 and 1:1, respectively. All five of the catalysts showed favorable catalytic activity for the three reactions at high temperatures (750–850 °C), which may be attributable to the relatively strong interaction between the NiO and the support. However, a decrease in the operational temperature led to different activities. Table 1 lists the detailed methane conversion over the five catalysts at 600 °C. It shows that the catalytic activities of the CeNi–Al_2O_3 and SmNi–Al_2O_3 catalysts were a little lower than those of the PrNi–Al_2O_3, LaNi–Al_2O_3 and GdNi–Al_2O_3 catalysts. For example, the CH_4 conversion over the GdNi–Al_2O_3 catalyst reached 86.2, 77.7 and 75.4% for the methane partial oxidation, steam and

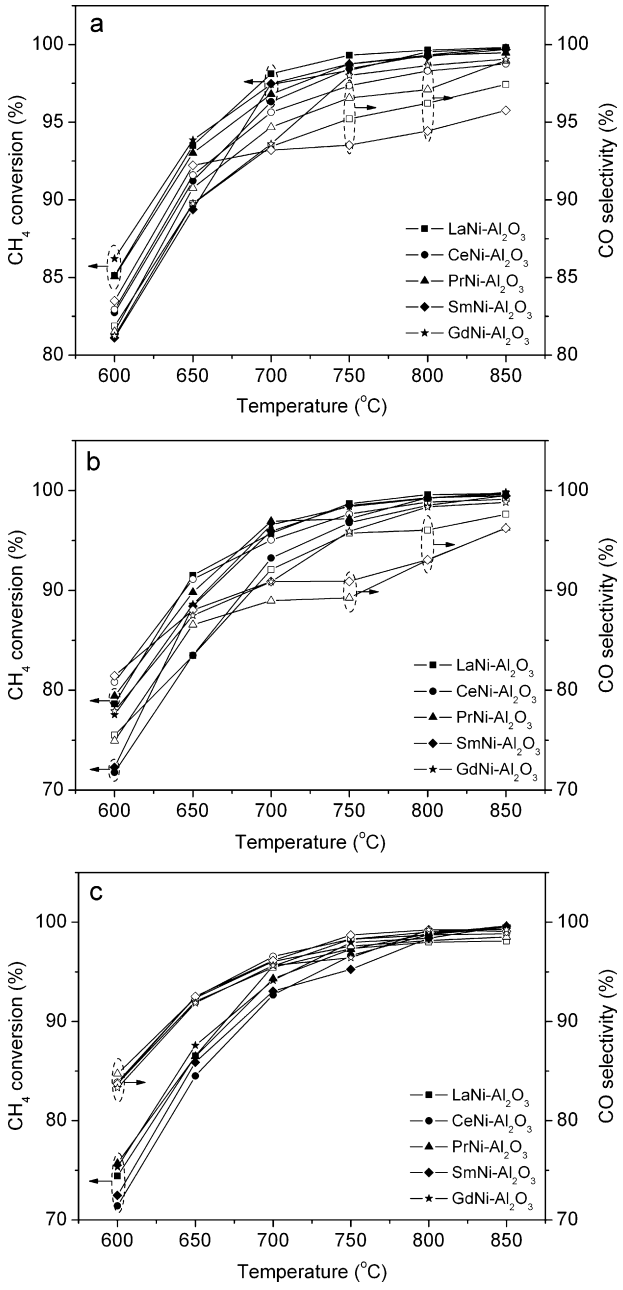

Fig. 3. The catalytic activity of the LaNi–Al_2O_3, CeNi–Al_2O_3, PrNi–Al_2O_3, SmNi–Al_2O_3, GdNi–Al_2O_3 catalysts for (a) partial oxidation (CH_4:O_2 = 2:1), (b) steam reforming (CH_4:H_2O = 1:1) and (c) CO_2 reforming (CH_4:CO_2 = 1:1) (solid symbol: CH_4 conversion; open symbol: CO selectivity).

Table 1
Methane conversion during the partial oxidation, steam reforming, and CO_2 reforming of methane at 600 °C over LaNi–Al_2O_3, CeNi–Al_2O_3, SmNi–Al_2O_3, PrNi–Al_2O_3 and GdNi–Al_2O_3.

Catalysts	CH_4 conversion		
	Partial oxidation	Steam reforming	CO_2 reforming
LaNi–Al_2O_3	85.1%	78.6%	74.4%
CeNi–Al_2O_3	82.7%	71.8%	71.4%
PrNi–Al_2O_3	85.0%	79.4%	75.7%
SmNi–Al_2O_3	81.1%	72.3%	72.4%
GdNi–Al_2O_3	86.2%	77.7%	75.4%

Table 2
H_2 to CO ratios for the partial oxidation, steam reforming, and CO_2 reforming of methane at 600–850 °C over LaNi–Al_2O_3, CeNi–Al_2O_3, PrNi–Al_2O_3, SmNi–Al_2O_3 and GdNi–Al_2O_3.

Catalyst	Temperature (°C)	H_2 to CO ratios		
		Partial oxidation	Steam reforming	CO_2 reforming
LaNi–Al_2O_3	850	2.07	3.09	1.03
	800	2.11	3.16	1.03
	750	2.14	3.17	1.04
	700	2.19	3.34	1.05
	650	2.26	3.79	1.01
	600	2.45	4.30	1.03
CeNi–Al_2O_3	850	2.02	3.03	1.02
	800	2.03	3.04	1.01
	750	2.06	3.10	1.00
	700	2.09	3.21	0.99
	650	2.17	3.39	0.98
	600	2.36	3.95	0.99
PrNi–Al_2O_3	850	2.02	3.15	1.03
	800	2.08	3.29	1.02
	750	2.09	3.48	1.02
	700	2.13	3.49	1.02
	650	2.22	3.62	1.01
	600	2.46	4.33	1.03
SmNi–Al_2O_3	850	2.13	3.15	1.01
	800	2.17	3.29	1.00
	750	2.19	3.40	0.97
	700	2.19	3.40	1.00
	650	2.12	3.54	0.99
	600	2.31	3.91	1.01
GdNi–Al_2O_3	850	2.02	3.04	1.01
	800	2.03	3.06	1.00
	750	2.04	3.17	1.05
	700	2.18	3.40	1.03
	650	2.27	3.57	1.03
	600	2.50	4.13	1.05

CO_2 reforming reactions, respectively, while they were 82.7, 71.8 and 71.4%, respectively, over the CeNi–Al_2O_3 catalyst.

The H_2 to CO ratio is an important factor to evaluate the catalysts during the syngas production reactions of methane [41–46]. The H_2 to CO ratios of the five catalysts in the methane partial oxidation, steam and CO_2 reforming reactions in this study are listed in Table 2. The H_2 to CO ratios of all the catalysts at 750–850 °C were near the theoretical values of 2.0, 3.0 and 1.0 for the methane partial oxidation, steam reforming and CO_2 reforming reactions, respectively. The H_2 to CO ratios could meet the different requirements for the production of many chemicals, such as HCHO and CH_3COOH. The H_2 to CO ratios increased with decreasing reaction temperatures for the methane partial oxidation and steam reforming reactions and the H_2 to CO ratio almost remained stable for the CO_2 reforming reaction. Liu et al. have reported similar results for the methane partial oxidation reaction [45]. Daza et al. have demonstrated that the H_2 to CO ratios almost remained stable for the CO_2 reforming reaction, which agrees with our results [46].

3.3. Carbon deposition

The catalyst stability for the methane conversion is closely related to the coke formation. Previously, we have demonstrated that the LiLaNi–Al_2O_3 (7 wt.% Ni) catalyst had better coke resistance than the Ni–Al_2O_3 [32]. The carbon deposition behavior of the lanthanide-promoted Ni–Al_2O_3 catalysts was then investigated. Fig. 4 shows the corresponding O_2-TPO profiles of the catalysts after treatment in methane at 850 °C. The CO_2 peak areas were 1.76×10^{-6}, 1.98×10^{-6}, 2.35×10^{-6}, 1.44×10^{-6}, 1.23×10^{-6} and 5.63×10^{-6} for LaNi–Al_2O_3, CeNi–Al_2O_3, PrNi–Al_2O_3, SmNi–Al_2O_3, GdNi–Al_2O_3 and Ni–Al_2O_3, respectively. The area of the CO_2 peak reflects the amount of carbon deposited on the catalysts, which was quantitatively determined by applying pure $SrCO_3$ as an external standard substance. Table 3 shows the area-specific carbon formation rates over the various catalysts. These results indicated that the introduction of lanthanides to the Ni–Al_2O_3 catalyst increased the coking resistance. The GdNi–Al_2O_3 catalyst had the best coking resistance. It is interesting that CeNi–Al_2O_3 was very different from the other four catalysts. This phenomenon may be because the CeO_2 did not enter the bulk phase in the catalyst, as evidenced by the XRD and TPR characterizations. The coke resistance regulation in the LaNi–Al_2O_3, PrNi–Al_2O_3, SmNi–Al_2O_3 and GdNi–Al_2O_3 catalysts agreed with the ionic radius of the corresponding promoter elements. Some promoters could create a steric effect, such as blocking certain catalytic sites or the adsorption/desorption modes of specific molecular geometries on the surface of the catalyst. The amount of deposited carbon also depended on the difference between the carbenium adsorption and desorption rates. The amount of adsorbed carbenium was controlled by the thermodynamic process. The desorption rate of the carbenium on the catalyst should be affected by the structure of the catalyst. It has been reported that the carbon deposition property of the supported catalyst is related to the steric hindrance of the catalyst [47]. The Gd^{3+} had the smallest ionic radius of 0.94 Å of the five elements in this study and the good coke resistance of GdNi–Al_2O_3 should be attributable to the steric effect of the promoter.

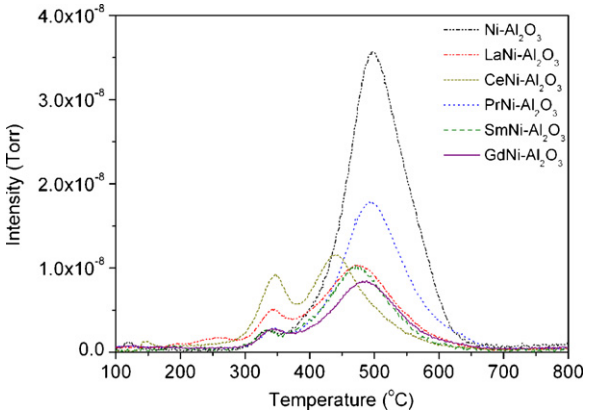

Fig. 4. The O_2-TPO profiles of the LaNi–Al_2O_3, CeNi–Al_2O_3, PrNi–Al_2O_3, SmNi–Al_2O_3 and GdNi–Al_2O_3 catalysts after treatment in pure methane for 5 min at 850 °C.

To investigate the structures of the deposited carbon, the laser Raman spectroscopy of the five carbon-deposited samples were measured. As shown in Fig. 5, the Raman spectra showed two intense bands, with the first one at 1350 cm^{-1} (usually called the D-band) associated with the disorder structure of carbon and the second one at 1580 cm^{-1} (usually called the G-band) assigned to the in-plane vibrations of the carbon atoms in hexagonal sheets [48]. The graphitization degree of the deposited carbon was related to the integrated intensity ratio in the form of R (I_D/I_G) [49]. According to the literature, the R-values should decrease with the increasing carbon graphitization degree [50]. The R-values of the deposited

Table 3
BET and carbon formation rates of the various catalysts under methane atmosphere.

Catalysts	BET ($m^2\ g^{-1}$)	Carbon formation rate (10^{-5} mol m^{-2} min^{-1})
LaNi–Al_2O_3	51.3	1.20
CeNi–Al_2O_3	69.5	1.00
PrNi–Al_2O_3	79.0	1.05
SmNi–Al_2O_3	52.7	0.97
GdNi–Al_2O_3	56.2	0.77
Ni–Al_2O_3	68.3	2.92

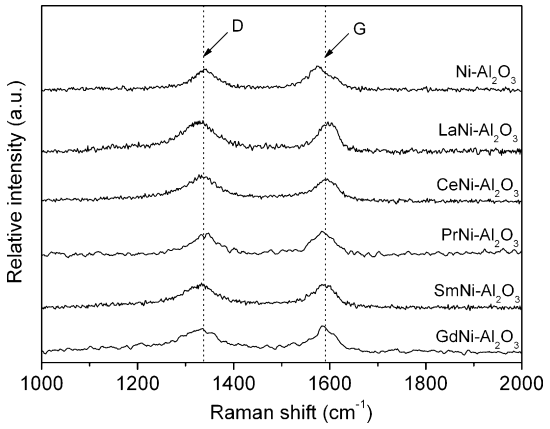

Fig. 5. The Raman spectra of the LaNi–Al_2O_3, CeNi–Al_2O_3, PrNi–Al_2O_3, SmNi–Al_2O_3 and GdNi–Al_2O_3 catalysts after treatment in pure methane for 5 min at 850 °C.

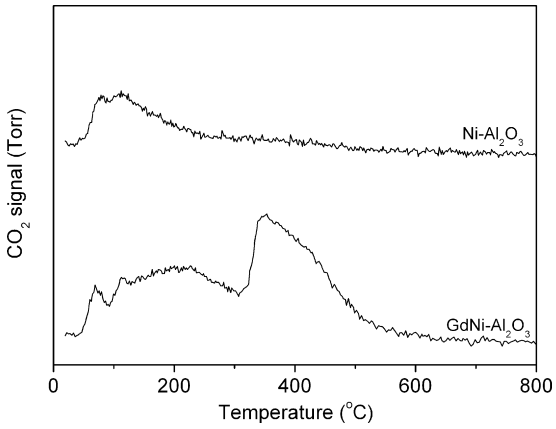

Fig. 7. The CO_2-TPD profiles of the Ni–Al_2O_3 and GdNi–Al_2O_3 catalysts after treatment in pure CO_2 for 2 h at room temperature.

carbon over the LaNi–Al_2O_3, CeNi–Al_2O_3, PrNi–Al_2O_3, SmNi–Al_2O_3, GdNi–Al_2O_3 and Ni–Al_2O_3 at 850 °C were 1.63, 1.32, 1.38, 1.21, 1.05 and 0.86, respectively. These findings indicate that the addition of various lanthanides could effectively decrease the graphitization degree of the carbon deposited over the catalysts.

To further exploit the coke resistance of the GdNi–Al_2O_3 catalyst, the catalyst was treated in pure methane at various temperatures and then subjected to the O_2-TPO analysis. Fig. 6 presents the O_2-TPO profiles of the GdNi–Al_2O_3 catalyst after treatment in methane at 650–850 °C. The CO_2 peak areas were 1.23×10^{-6}, 2.52×10^{-6}, 3.60×10^{-6}, 7.85×10^{-6}, 1.10×10^{-5} at 850, 800, 750, 700 and 650 °C, respectively. The area-specific carbon formation rates of the corresponding temperatures were 7.70×10^{-6}, 1.58×10^{-5}, 2.26×10^{-5}, 4.92×10^{-5} and 6.90×10^{-5} mol m^{-2} min^{-1}, respectively. These results indicate an increase in the coke formation rate with a decrease in the reaction temperature for the GdNi–Al_2O_3 catalyst. Based on the hydrocarbon cracking reaction thermodynamics, an increase in the reaction temperature should not cause a decrease in the rate of coke formation. However, coke is the product of the inter-reactions between carbenium ions on the catalyst surface. Thus, due to an increase in the desorption rate, fewer carbenium ions were present on the catalyst surface at high temperatures. As a result, the rate of coke formation decreased with an increase in temperature [51].

It is well known that an acidic catalyst surface favors carbon deposition, while a basic one suppresses carbon deposition [52]. To test the surface basicity of the lanthanide-promoted Ni–Al_2O_3 catalysts, the CO_2-TPD process was performed. Fig. 7 shows the corresponding CO_2-TPD profiles of the GdNi–Al_2O_3 and Ni–Al_2O_3 catalysts. No absorption peak existed at the region above 600 °C, which implied that no carbonate was produced in our CO_2-TPD process. The CO_2 peak areas were 1.22×10^{-7} and 4.53×10^{-7} for the Ni–Al_2O_3 and GdNi–Al_2O_3, respectively. Thus, the GdNi–Al_2O_3 catalyst had a higher surface basicity than the Ni–Al_2O_3. This result showed that the good coke resistance of the GdNi–Al_2O_3 should be attributable to the steric effect of the Gd_2O_3 promoter and the large surface basicity of the catalyst.

3.4. Long-term catalyst stability

To evaluate the operational stability, the GdNi–Al_2O_3 catalyst was tested for methane partial oxidation under the conditions of CH_4:O_2 = 2:1 at 850 °C for a period of 300 h. Fig. 8 shows the corresponding methane conversion and the H_2 to CO ratio. The methane conversion was stable at approximately 99% and the H_2 to CO ratio stayed around 2.0 during the 300 h operation. The catalytic deactivation of the γ-Al_2O_3-supported catalysts during high-temperature operations is typically due to the thermal deterioration of the γ-Al_2O_3 support, i.e., the sintering and phase transformation into the low-surface area α-Al_2O_3 [53]. Rare earth metal oxides could prevent the alumina support from thermal deterioration [54]. The rare earth oxides also have a high oxygen storage capacity and can absorb or release oxygen reversibly in response to the oxygen concentration in the gas-phase [55]. Their presence shows beneficial effects on the catalyst performance, such as improving the dispersion of the active species and delaying the transition of the alumina support from γ-Al_2O_3 to α-Al_2O_3 [56,57]. The strong interaction between the NiO species and the Al_2O_3, the good coking resistance

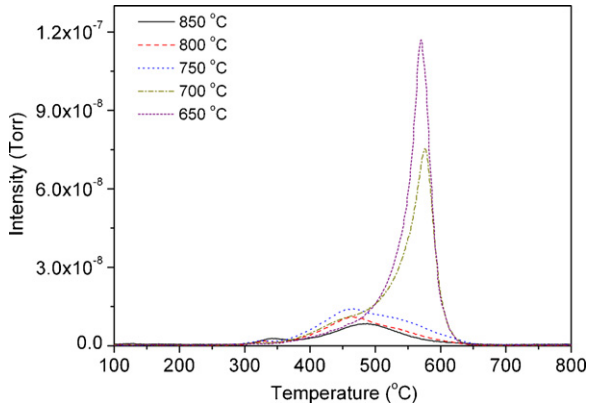

Fig. 6. The O_2-TPO profiles of the GdNi–Al_2O_3 catalyst after treatment in pure methane for 5 min at 650–850 °C.

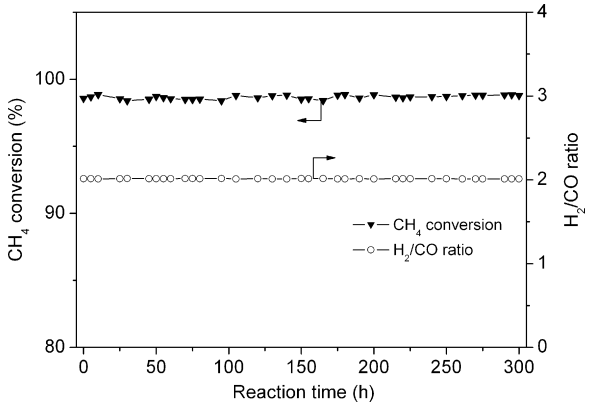

Fig. 8. The time dependence of methane conversion and the H_2 to CO ratio under CH_4:O_2 = 2:1 conditions at 850 °C for the GdNi–Al_2O_3 catalyst.

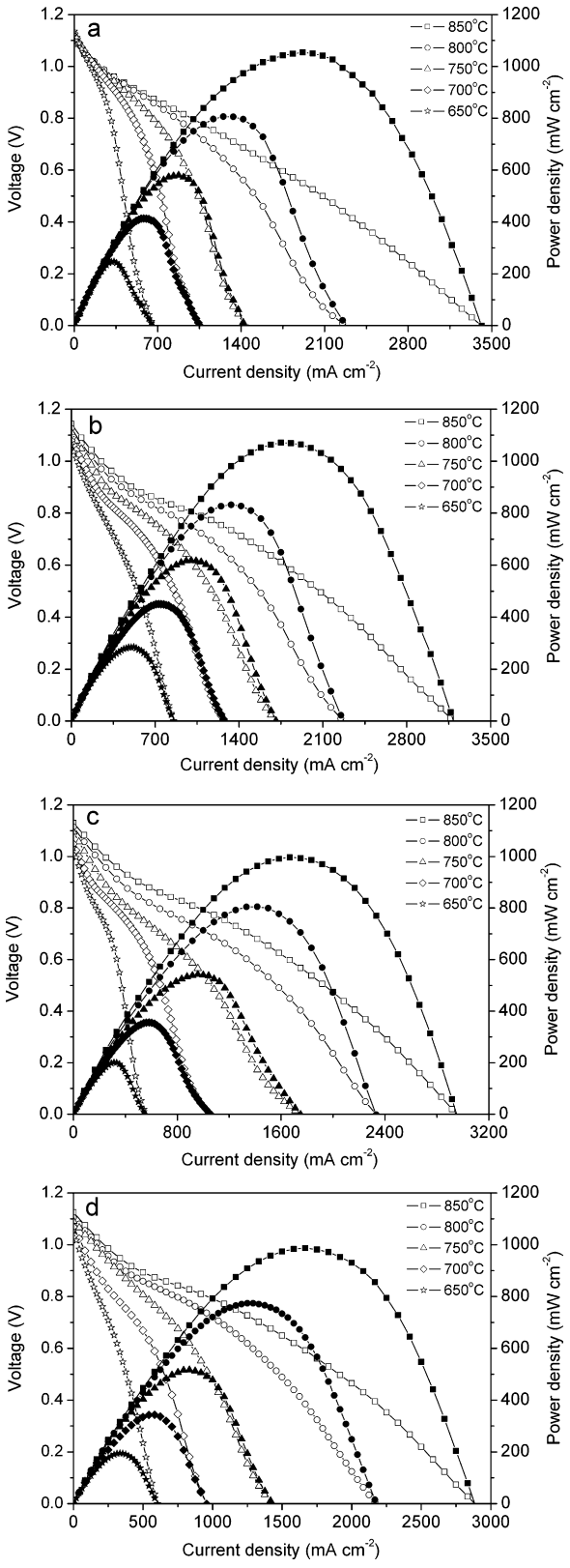

Fig. 9. The *I–V* and *I–P* curves of the fuel cells with the GdNi–Al_2O_3 catalyst layer operating on a mixed gas composed of (a) pure hydrogen, (b) 80% CH_4 and 20% O_2, (c) 66.7% CH_4 and 33.3% H_2O, and (d) 66.7% CH_4 and 33.3% CO_2 at different temperatures.

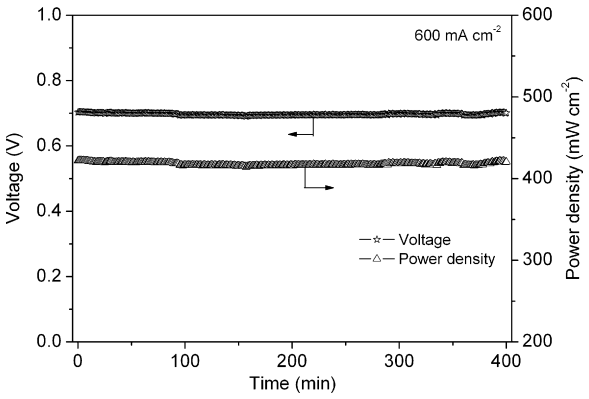

Fig. 10. The time dependence of the voltage and power density under a specific current density (600 mA cm^{-2}) at 750 °C of the fuel cell with the GdNi–Al_2O_3 catalyst layer operating on methane–oxygen gas mixtures as fuel.

and the high surface basicity of GdNi–Al_2O_3, as evidenced by the H_2-TPR, O_2-TPO and CO_2-TPD results, largely contributed to the excellent stability of the GdNi–Al_2O_3 catalyst.

3.5. Single cell performance

The GdNi–Al_2O_3 catalyst was then investigated as the anode functional layer in a single cell. Fig. 9 shows the *I–V* and *I–P* curves of the fuel cell operating on a methane–O_2 gas mixture, a methane–H_2O gas mixture and a methane–CO_2 gas mixture. The methane to O_2, H_2O and CO_2 ratios were 4:1, 2:1 and 2:1, respectively. By applying the methane–O_2 gas mixtures as the fuel, the cell delivered peak power densities of 1068, 832, 618, 450 and 285 mW cm^{-2} at 850, 800, 750, 700 and 650 °C, respectively, while they were 1054, 805, 580, 413 and 247 mW cm^{-2} when pure hydrogen was applied as the fuel. These results showed that the cell power outputs were similar for operating on methane–O_2 fuel and hydrogen fuel. The cell delivered similar power outputs by operating on methane–H_2O or methane–CO_2 gas mixtures. For example, the peak power densities at 850 °C were 996 or 986 mW cm^{-2} when methane–H_2O or methane–CO_2 gas mixtures served as fuels, respectively. These results indicate that the catalyst layer had suf-

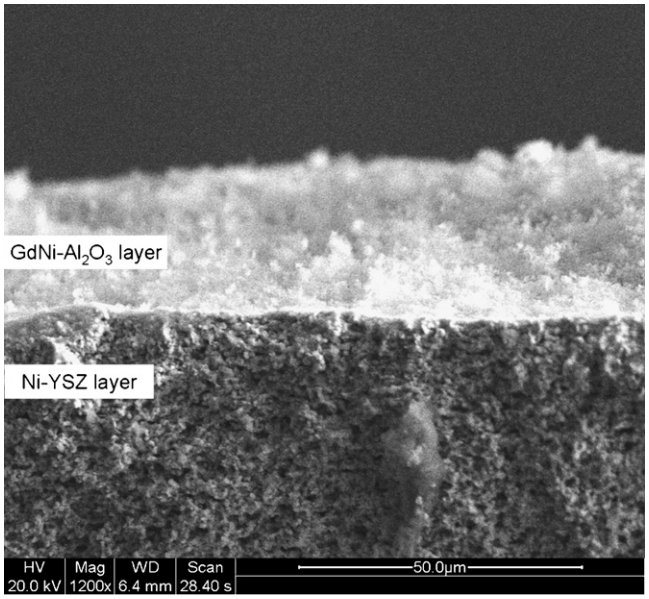

Fig. 11. The cross-sectional SEM images of the GdNi–Al_2O_3 catalyst–anode interface after the cell performance and stability test.

ficient catalytic activity for the partial oxidation, steam reforming and CO_2 reforming of methane.

The cell stability with the GdNi–Al_2O_3 catalyst layer under a specific current density at 750 °C was then investigated. As shown in Fig. 10, methane–O_2 gas mixtures (CH_4:O_2 = 4:1) were investigated as the cell fuel. Under a current density of 600 mA cm^{-2}, the voltage was stable at about 0.70 V during the entire 400 min test and the corresponding power density was stable at about 420 mW cm^{-2}. This good stability should contribute to the excellent coking resistance of the GdNi–Al_2O_3 catalyst, as evidenced by the O_2-TPO results.

The SEM image of the fuel cell after the cell performance and stability test between 650 and 850 °C under different fuel conditions for a period of 15 h is shown in Fig. 11. The catalyst layer still adhered to the anode surface fairly well. The above results indicate that the coking resistant GdNi–Al_2O_3 catalyst can be used as the functional layer of SOFCs operating on methane fuel.

4. Conclusions

The combustion-synthesized lanthanide-promoted Ni–Al_2O_3 catalysts had good catalytic activity for the partial oxidation, steam reforming and CO_2 reforming of methane at elevated temperatures. The catalytic activity of the GdNi–Al_2O_3 was comparable to those of the LaNi–Al_2O_3 and PrNi–Al_2O_3 catalysts but was higher than those of the CeNi–Al_2O_3 and SmNi–Al_2O_3 catalysts. The strong interaction between the NiO and the support accounted for the high activity of the catalysts. The GdNi–Al_2O_3 catalyst also presented the best coke resistance under pure methane conditions among all of the catalysts, and it remained stable under the conditions of CH_4:O_2 = 2:1 for 300 h at 850 °C. A fuel cell with a GdNi–Al_2O_3 catalyst layer yielded high cell performance when operating on methane–O_2, methane–H_2O or methane–CO_2 gas mixtures. The cell with the GdNi–Al_2O_3 catalyst layer was stable when operating on methane–O_2 mixtures at 750 °C for 400 min. The excellent catalytic activity and stability and the high coking resistance of GdNi–Al_2O_3 indicate a promising application as the catalyst layer in SOFCs operating on methane.

Acknowledgements

This work was supported by the “National Science Foundation for Distinguished Young Scholars of China” under contract No. 51025209, by the “Outstanding Young Scholar Grant at Jiangsu Province” under contract No. 2008023, by the program for New Century Excellent Talents (2008), and by the Fok Ying Tung Education Foundation under contract No. 111073.

References

[1] I. Wender, Fuel Process. Technol. 48 (1996) 189–297.
[2] W. Zhou, Z.P. Shao, R. Ran, W.Q. Jin, N.P. Xu, Chem. Commun. 44 (2008) 5791–5793.
[3] T. Hibino, A. Hashimoto, T. Inoue, J. Tokuno, S. Yoshida, M. Sano, Science 288 (2000) 2031–2033.
[4] A. Wojcik, H. Middleton, I. Damopoulos, J. Van herle, J. Power Sources 118 (2003) 342–348.
[5] Y.Z. Wu, C. Su, C.M. Zhang, R. Ran, Z.P. Shao, Electrochem. Commun. 11 (2009) 1265–1268.
[6] C. Su, Y.Z. Wu, W. Wang, Y. Zheng, R. Ran, Z.P. Shao, J. Power Sources 195 (2010) 1333–1343.
[7] S.P. Jiang, S.H. Chan, Mater. Sci. Technol. 20 (2004) 1109–1118.
[8] S.P. Jiang, S.H. Chan, J. Mater. Sci. 39 (2004) 4405–4439.
[9] C. Lu, W.L. Worrell, J.M. Vohs, R.J. Gorte, J. Electrochem. Soc. 150 (2003) A1357–A1359.
[10] H.P. He, J.M. Vohs, R.J. Gorte, J. Electrochem. Soc. 150 (2003) A1470–A1475.
[11] Y.H. Huang, R.I. Dass, Z.L. Xing, J.B. Goodenough, Science 312 (2006) 254–257.
[12] S.W. Tao, J.T.S. Irvine, Nat. Mater. 2 (2002) 320–323.
[13] Z.L. Zhan, Y.B. Lin, M. Pillai, I. Kim, S.A. Barnett, J. Power Sources 161 (2006) 460–465.
[14] Z.L. Zhan, S.A. Barnett, Solid State Ionics 176 (2005) 871–879.
[15] Z.L. Zhan, S.A. Barnett, Science 308 (2005) 844–847.
[16] A.T. Ashcroft, A.K. Cheetham, M.L.H. Green, P.D.F. Vernon, Nature 352 (1991) 225–226.
[17] P.D.F. Vemon, M.L.H. Green, A.K. Cheetham, A.T. Ashcroft, Catal. Today 13 (1992) 417–426.
[18] K. Asami, X.H. Li, K. Fujimoto, Y. Koyama, A. Sakurama, N. Kometani, Y. Yonezawa, Catal. Today 84 (2003) 27–31.
[19] Q.G. Yan, T.H. Wu, W.Z. Weng, H. Toghiani, R.K. Toghiani, H.L. Wan, C.U. Pittman Jr., J. Catal. 226 (2004) 247–259.
[20] D. San-José-Alonso, J. Juan-Juan, M.J. Illán-Gómez, M.C. Román-Martínez, Appl. Catal. A: Gen. 371 (2009) 54–59.
[21] W. Wang, W. Zhou, R. Ran, R. Cai, Z.P. Shao, Electrochem. Commun. 11 (2009) 194–197.
[22] W. Wang, C. Su, Y.Z. Wu, R. Ran, Z.P. Shao, J. Power Sources 195 (2010) 402–411.
[23] S.B. Wang, G.Q. (Max) Lu, J. Chem. Technol. Biotechnol. 75 (2000) 589–595.
[24] Q. Zhuang, Y.N. Qin, L. Chang, Appl. Catal. 70 (1991) 1–8.
[25] S.B. Wang, G.Q. (Max) Lu, Appl. Catal. B: Environ. 19 (1998) 267–277.
[26] S. Natesakhawat, R.B. Watson, X.Q. Wang, U.S. Ozkan, J. Catal. 234 (2005) 496–508.
[27] N. Laosiripojana, W. Sutthisripok, S. Assabumrungrat, Chem. Eng. J. 112 (2005) 13–22.
[28] L.Y. Mo, X.M. Zheng, Q.S. Jing, H. Lou, J.H. Fei, Energy Fuels 19 (2005) 49–53.
[29] S. Natesakhawat, O. Oktar, U.S. Ozkan, J. Mol. Catal. A: Chem. 241 (2005) 133–146.
[30] J. Gao, Z.Y. Hou, J.Z. Guo, Y.H. Zhu, X.M. Zheng, Catal. Today 131 (2008) 278–284.
[31] R.Q. Yang, C. Xing, C.X. Lv, L. Shi, N. Tsubaki, Appl. Catal. A: Gen. 385 (2010) 92–100.
[32] W. Wang, R. Ran, Z.P. Shao, J. Power Sources 196 (2011) 90–97.
[33] W. Wang, R. Ran, Z.P. Shao, Int. J. Hydrogen Energy, doi:10.1016/j.ijhydene.2010.09.048, in press.
[34] H.X. Gu, R. Ran, W. Zhou, Z.P. Shao, J. Power Sources 172 (2007) 704–712.
[35] W.Q. Zheng, J. Zhang, Q.J. Ge, H.Y. Xu, W.Z. Li, Appl. Catal. B: Environ. 80 (2008) 98–105.
[36] X.Y. Chen, Y. Liu, G.X. Niu, Z.X. Yang, M.Y. Bian, A.D. He, Appl. Catal. A: Gen. 205 (2001) 159–172.
[37] L.P. Haack, C.R. Peters, J.E. deVries, K. Otto, Appl. Catal. A: Gen. 87 (1992) 103–114.
[38] H.S. Roh, K.W. Jun, Catal. Surv. Asia 12 (2008) 239–252.
[39] J.Z. Guo, Z.Y. Hou, J. Gao, X.M. Zheng, Fuel 87 (2008) 1348–1354.
[40] S.D. Robertson, B.D. McNicol, H. De Bass, S.C. Kloet, J.W. Jenkins, J. Catal. 37 (1975) 424–431.
[41] V.R. Choudhary, A.M. Rajput, B. Prabhakar, A.S. Mamman, Fuel 77 (1998) 1803–1807.
[42] W. Wang, S.M. Stagg-Williams, F.B. Noronha, L.V. Mattos, F.B. Passos, Catal. Today 98 (2004) 553–563.
[43] M.M.V.M. Souza, M. Schmal, Appl. Catal. A: Gen. 281 (2005) 19–24.
[44] Q.S. Jing, X.M. Zheng, Energy 31 (2006) 2184–2192.
[45] Y. Liu, F.Y. Huang, J.M. Li, W.Z. Weng, C.R. Luo, M.L. Wang, W.S. Xia, C.J. Huang, H.L. Wan, J. Catal. 256 (2008) 192–203.
[46] C.E. Daza, C.R. Cabrera, S. Moreno, R. Molina, Appl. Catal. A: Gen. 378 (2010) 125–133.
[47] A. Monzon, G. Lolli, S. Cosma, S.B. Mohamed, D.E. Resasco, J. Nanosci. Nanotechnol. 8 (2008) 6141–6152.
[48] F. Tuinstra, J.L. Koenig, J. Chem. Phys. 53 (1970) 1126–1130.
[49] A. Cuesta, P. Dhamelincourt, J. Laureyns, A. Martínez-Alonso, J.M.D. Tascón, Carbon 32 (1994) 1523–1532.
[50] P. Lespade, A. Marchand, M. Couzi, F. Cruege, Carbon 22 (1984) 375–385.
[51] Y.X. Zhao, F. Wei, Y. Yu, AIChE J. 54 (2008) 750–755.
[52] S.B. Tang, F.L. Qiu, S.J. Lu, Catal. Today 24 (1995) 253–255.
[53] W.G. Schlaffer, C.Z. Morgan, J.N. Wilson, J. Phys. Chem. 61 (1957) 714–722.
[54] M. Pijolat, M. Dauzat, M. Soustelle, Solid State Ionics 50 (1992) 31–39.
[55] H.C. Yao, Y.F.Y. Yao, J. Catal. 86 (1984) 254–265.
[56] J. Soria, J.M. Coronado, J.C. Conesa, J. Chem. Soc., Faraday Trans. 92 (1996) 1619–1626.
[57] C. Morterra, V. Bolis, G. Magnacca, J. Chem. Soc., Faraday Trans. 92 (1996) 1991–1999.